

THRESHOLD ERROR RATES FOR THE TORIC AND SURFACE CODES

D. S. WANG^a, A. G. FOWLER, A. M. STEPHENS, L. C. L. HOLLENBERG

*Centre for Quantum Computer Technology,
School of Physics, University of Melbourne,
Victoria 3010, Australia*

Abstract

The surface code scheme for quantum computation features a 2d array of nearest-neighbor coupled qubits yet claims a threshold error rate approaching 1% [1]. This result was obtained for the toric code, from which the surface code is derived, and surpasses all other known codes restricted to 2d nearest-neighbor architectures by several orders of magnitude. We describe in detail an error correction procedure for the toric and surface codes, which is based on polynomial-time graph matching techniques and is efficiently implementable as the classical feed-forward processing step in a real quantum computer. By direct simulation of this error correction scheme, we determine the threshold error rates for the two codes (differing only in their boundary conditions) for both ideal and non-ideal syndrome extraction scenarios. We verify that the toric code has an asymptotic threshold of $p_{\text{th}} = 15.5\%$ under ideal syndrome extraction, and $p_{\text{th}} = 7.8 \times 10^{-3}$ for the non-ideal case, in agreement with [1]. Simulations of the surface code indicate that the threshold is close to that of the toric code.

1 Introduction

Quantum computation is the manipulation of quantum information, typically in the form of *qubits*, the quantum analogue of the classical bit [2]. Qubits differ fundamentally from their classical counterparts as they can be placed in arbitrary superpositions of their basis states: $\alpha |0\rangle + \beta |1\rangle$. This freedom allows for novel new prospects in computation, as demonstrated by the existence of quantum algorithms outperforming existing classical algorithms [3, 4]. Quantum algorithms must necessarily make use of superposition states and entanglement to be distinguishable from, and potentially outperform, classical algorithms. Thus the preservation of the quantum state is crucial. Interactions with the environment (decoherence) will inevitably occur, altering the fragile quantum state thus leading to unreliable output. Quantum error correction [5–7] may be employed to counteract this.

Error correction makes use of redundant information in order to correct for physical errors; the higher the redundancy, the more locations for errors and yet simultaneously the more

^adswang@physics.unimelb.edu.au

errors that can be corrected. The balance between increased errors and corrective ability gives rise to a threshold error rate [8], below which error correction reduces the effective error rate. If all physical gates are constructed with a failure rate below this threshold error rate, quantum error correction enables arbitrary length quantum computation to be achieved. In the case of the surface codes, logical qubits are created from pairs of holes in a lattice of qubits. One logical operation is a chain of physical operations connecting together pairs of holes, the other is a ring encompassing one hole. The minimum number of errors required to cause logical failure can be increased by increasing the separation between holes and the circumference around holes, thus the logical error rate is exponentially suppressed assuming random independent errors.

Threshold error rates are highly dependent on the underlying assumptions. For example, given long-range interactions and a very large number of qubits, one finds the threshold for fault-tolerant computation to be over 3% [9]. At the other end of the scale, if one assumes the most restrictive arrangement, a linear nearest-neighbor architecture, the threshold is approximately 10^{-5} [10].

More recently, the toric code [11] has kindled interest. The original scheme arranges a 2d array of nearest-neighbor coupled qubits on the surface of a torus which may be mapped onto a simple 2d plane with periodic boundary conditions (figure 1a). Computation on the toric code has since been extended to the surface code which foregoes the need for periodic boundary conditions [1, 12, 13], relaxing the demands imposed on physical realization. In this paper, we will distinguish the *toric code* as originally conceived by Kitaev from this extended 2d *surface code* with its hard boundaries.

The toric code threshold computed in [1] was surprisingly high, $p_{\text{th}} = 7.5 \times 10^{-3}$. In comparison, given the same 2d nearest-neighbor physical architecture, the concatenated 7-qubit Steane code has a threshold of 1.85×10^{-5} [14], while the concatenated Bacon-Shor code has a threshold of 2.02×10^{-5} [15]. In order to verify the toric code threshold, we simulate the average time a logical qubit encoded in either code retains its logical state using error correction procedures one can implement in practice. Note that classical computation is required to diagnose the errors from the quantum circuits in a real life quantum computer, and that the error correction methodology applied in our simulations is applicable without modification to a real quantum computer.

Since the two codes differ only in their boundary conditions, one expects that the asymptotic threshold for the surface code to be identical to the toric code but this has yet to be numerically demonstrated. We justify this claim for when the syndrome extraction circuits are error-free (*ideal*) and error-prone (*non-ideal*). We show that the toric code has an asymptotic threshold of $p_{\text{th}} = 15.5\%$ under ideal syndrome extraction, and $p_{\text{th}} = 7.8 \times 10^{-3}$ for the non-ideal case, coinciding with [1]. In both cases, the surface code threshold lies in the vicinity of this value.

This paper is organized as follows. Section 2 briefly reviews the toric code and the surface code. Section 3 presents the syndrome extraction circuits used throughout the simulations. An efficient method to correct errors is described in section 4. We also discuss several optimizations rendering the method more practical. Section 5 describes the simulation details, and results from the toric code and the surface code simulations are contrasted.

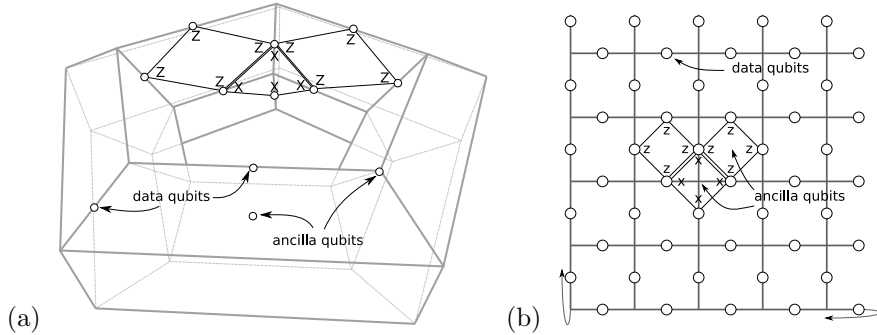


Fig. 1. (a) Toric code qubit arrangement shown in 3d. (b) Equivalent lattice represented in 2d with periodic boundaries. Stabilizer generators are the tensor products of the Pauli- Z and Pauli- X matrices around faces and intersections respectively.

2 The toric and surface codes

We introduce the essential elements of the toric and surface codes following the ideas of [16]. Consider a collection of qubits arranged on the surface of a torus as shown in figure 1a, or more easily represented as a regular 2d array of qubits with periodic boundary conditions (figure 1b). The qubits are divided into two categories: data qubits located on the lines of the grid, and ancilla qubits on the faces and the intersections.

The stabilizer generators for the toric code are the tensor products of the Pauli- Z matrices, Z , on the four data qubits around each face, and the tensor products of the Pauli- X matrices, X , on the four qubits around each intersection. Neighboring stabilizers share two data qubits ensuring that the X and Z -stabilizers commute. Using the ancilla qubits, the eigenvalues of these stabilizers may be measured whilst still preserving a quantum state. We will always assume that the computer is initialized to the simultaneous $+1$ eigenstate of every stabilizer.

An X -error on a data qubit anti-commutes with the two adjacent Z -stabilizers. Assuming no others errors occur, we observe a change in the measured eigenvalue of the adjacent Z -stabilizers, from $+1$ to -1 . Similarly, Z -errors result in changes in the measured eigenvalues of two adjacent X -stabilizers. In general, if many closely separated errors occur, one observes the *terminals* of chains of errors (figure 2).

The interspersed ancilla allow for these eigenvalues to be measured using only local interactions, via the circuits shown in figure 5. The configuration of eigenvalues measured by the ancilla on the faces forms the X -syndrome from which X -errors may be corrected. Similarly, Z -errors are corrected using syndrome information from ancilla located on the intersections. The details of how the syndrome is used to correct errors are presented in section 4.

Logical operations can be associated with the four *non-homotopic* closed paths around the torus which cannot be contracted to a single stabilizer generator, shown in figure 3. (Two paths are *homotopic* if one can be continuously deformed into the other, in this case by multiplying by stabilizers). This particular topology defines two logical qubits: one from $X_L^{(1)}$ and $Z_L^{(1)}$, the other from $X_L^{(2)}$ and $Z_L^{(2)}$. These closed rings always overlap at an odd number of sites, yielding the correct commutation relations between logical operations. The *distance* of a code, d , is the length of the shortest logical operation.

In the absence of long-range physical gates, this topological code is difficult to realize as

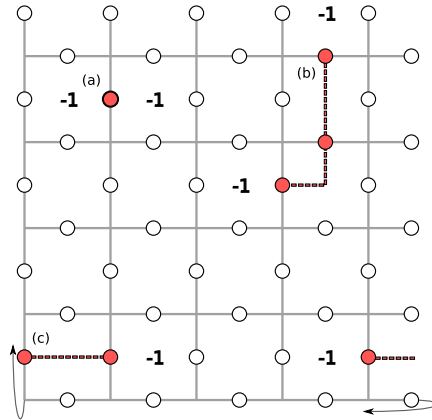


Fig. 2. The state is initialized to the +1 eigenstate of all stabilizers. Shaded qubits indicate locations of X -errors. (a) A single X -error toggles the eigenvalue measured in the adjacent faces in the next syndrome extraction cycle. Z -errors are similarly detected by the neighboring intersections. (b) When errors are closely spaced, one observes only the terminals of a continuous chain. (c) Error chains can wrap around the boundaries in the toric code, but not in the surface code.

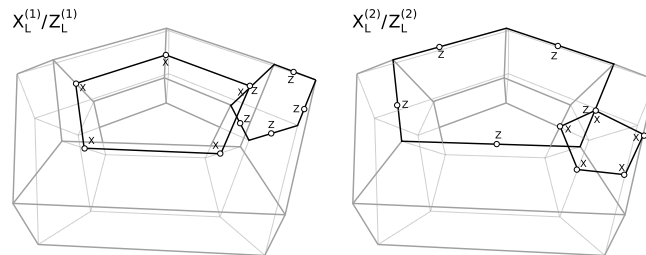


Fig. 3. Two logical- X and logical- Z operators in the toric code. Other rings of single-qubit X or Z operators on the lattice can either be deformed to products of the above rings, or contracted down to a single stabilizer generator.

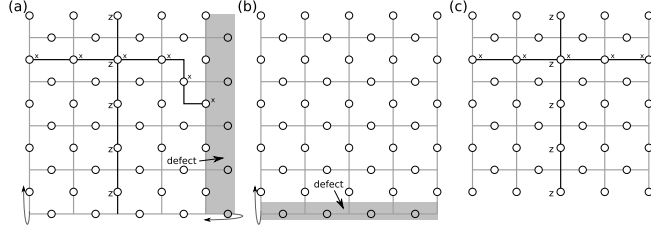


Fig. 4. (a) A smooth periodic defect is introduced into the toric code, eliminating one periodic boundary. The logical- X operation now becomes any chain of X operations connecting the left and right boundaries together. (b) A rough periodic defect is introduced to replace the remaining periodic boundary with a hard boundary. (c) The 2d surface code and its logical operations.

one would need to create a quasi-3d quantum computer. The surface code is a variation on the toric code, whereby the periodicity is removed [16]. The construction is most easily seen as the introduction of two *defects*: regions in the torus where ancilla qubits are no longer measured. Data qubits within the defect are no longer required and the stabilizers must be changed to reflect this. This process is illustrated in figure 4.

The first “smooth” defect cuts the torus into a cylinder. A smooth defect is a contiguous region of Z -stabilizer generators which we choose to ignore. In doing so, one eliminates a column of qubits and the horizontal periodicity. In addition, the $Z_L^{(2)}$ operation is lost, and the logical- X operation becomes any chain of X operations connecting the left and right boundaries together. Similarly, the vertical periodicity can be removed by introducing a “rough” defect — a defect associated with a contiguous region of X -stabilizer generators. This defect removes the $X_L^{(2)}$, so that there still remains one degree of freedom, defining a logical qubit. The end result is a code implementable on a regular 2d array of qubits with only local interactions. The construction of the surface code shown here will suffice for this paper. More detailed accounts can be found in [17, 18].

3 Syndrome extraction

Syndrome extraction on the toric code is done simultaneously for both X and Z syndromes. In our simulations, this is achieved using the circuits in figure 5. First, the ancilla qubits are prepared in their designated states. Then each ancilla interacts with the data qubits to its north, west, east and south (in that order). Finally, the ancilla are measured in the designated bases. This particular interaction order leads to ancilla qubits being in a simple product state at the end of the cycle, as each syndrome circuit can be shown to occur strictly before or after its neighboring syndrome circuits.

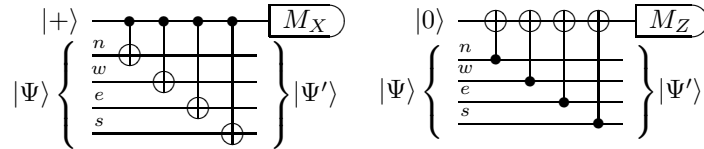


Fig. 5. Circuits used to measure X -stabilizers (left) and Z -stabilizers (right).

Since syndrome extraction is itself a physical process, it too is prone to errors. Under faulty syndrome extraction, error correction works in these schemes by collating the eigenvalue

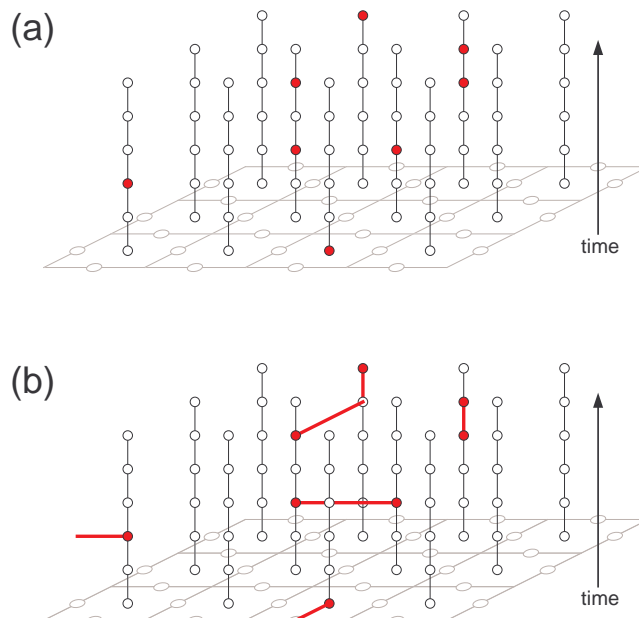


Fig. 6. (a) colored dots indicate the locations in space and time where the reported syndrome is different from that in the previous timestep. (b) Changes in syndrome mark the terminals of chains of errors, thus matching identifies a set of corrections to apply to correct the code.

measurements over the duration of the computation, forming a 3d syndrome structure (figure 6). The syndrome is now the *change* in eigenvalues measured between sequential timeslices, just as the syndrome for ideal syndrome extraction was the change from a $+1$ eigenvalue to a -1 eigenvalue. Error correction remains the task of finding the most likely set of errors that is consistent with the observed syndrome, which now is in 3-dimensions: two spatial and one temporal.

4 Error correction

The syndrome extracted gives us enough information to correct the state back to a codeword (ie. the simultaneous $+1$ eigenstate of all stabilizers), however we have yet to describe a method for doing this. Further, the method should be *efficient* (ie. runs in polynomial-time in the number of physical errors) for a quantum computer implementing this code to outperform classical computation. This condition prevents us from performing an exhaustive search to generate the observed syndrome as the search space grows exponentially with the lattice size.

One efficient method to error correct is by *matching*. A perfect matching on a graph is a subgraph in which every node in the graph has exactly one edge. Polynomial-time minimum-weight perfect matching algorithms exist based on Edmonds' blossom algorithm [19, 20].

We will first focus on the toric code, assuming ideal (error-free) syndrome extraction. The problem is first formed as a graph. The observed eigenvalue changes form the nodes on a graph. Each pair of nodes is connected by a weighted edge, which is associated with a chain of errors producing those two observed terminals. A perfect matching of the graph is then

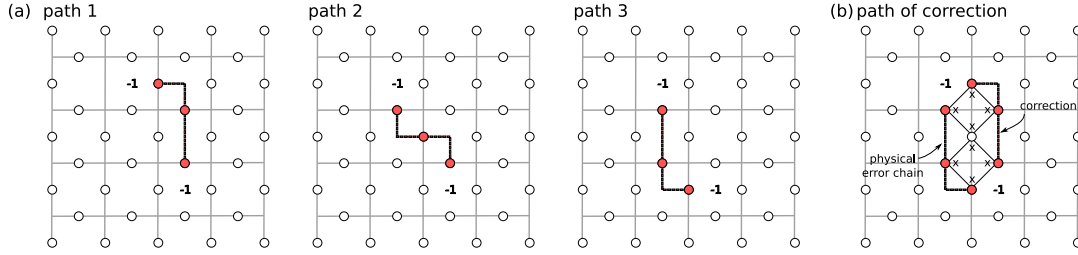


Fig. 7. (a) Three equally weighted error chains with identical syndromes. (b) The syndrome observed is due to physical errors on the data qubits along path 3. Unable to distinguish between the three options, we arbitrarily choose to correct along path 1. Since the resultant bit flips (including the physical errors) are a product of stabilizer generators, the original logical state is restored.

a set of error chains reproducing the syndrome. As there are many possible error chains linking any two nodes, we choose any of the possible chains of maximum probability. In our simulations, since all sites have equal probability of error, this equates to the shortest length error chains. An edge linking two nodes is assigned a weight equal to this shortest length. Thus a minimum-weight perfect matching reproduces the observed syndrome using the fewest errors. Since each edge in the matching represents one error chain, in order to error correct one applies corrections on the qubits along the error chains given by the matching.

Consider figure 7a, showing three different physical error chains producing identical syndromes. When such ambiguities arise, there is no way to distinguish which correction to apply. Suppose that we choose to always correct the qubits along path 1, but the physical errors occurred along path 3. Under ideal syndrome extraction, it can be shown that for fewer than $\lfloor (d+1)/2 \rfloor$ errors, any chain connecting the syndrome changes is homotopic to the physical error chain. In other words, such corrections will always form rings of errors, which are products of the stabilizer generators (figure 7b). Thus the logical state is restored.

Instead of each edge representing only one error chain, one could sum over all the different ways of generating the observed terminals and weigh it accordingly. While this has not been done, it could potentially improve the error correction procedure.

Generalising this method to incorporate errors during syndrome extraction is straightforward. Recall that it is the changes in eigenvalue measurements at the same location between sequential timeslices which contribute to the syndrome. These observed changes still mark the terminals of error chains, thus we can use the same formalism. They form the nodes in a graph, and weighted edges connect pairs of nodes.

A segment of an error chain spanning through time denotes an incorrect syndrome measurement, for example due to a preparation or a measurement error in the ancilla qubit. In practice, such errors may occur at different rates compared to data errors. One could then weigh time-separated segments of the error-chains differently to equivalent length space-separated error-chain segments in order to improve the performance of error correction. The ideal syndrome extraction limit is the specialised case where time-separated segments bear infinite weight, thereby severing nodes in one timeslice from nodes in other timeslices. In our simulations, we will take the simplistic option where space-separated and time-separated segments are weighted equally for a pessimistic threshold.

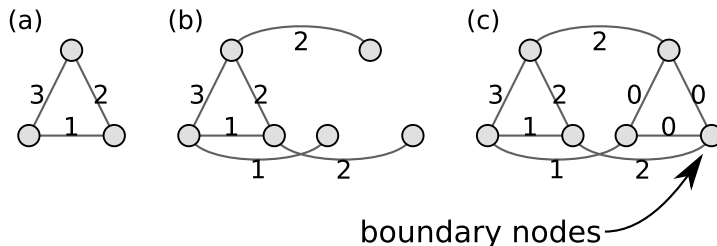


Fig. 8. (a) Graph as formed by toric code formulation does not account for boundaries. (b) Boundaries included, but matching this graph does not correct errors. (c) Final graph which, once matched, returns the desired correction.

During the final step of an algorithm, syndrome information is extracted by error free circuits so that the final syndrome measurement can always be assumed to be correct. Coupled with perfect initialisation, there will always be an even number of nodes ensuring a perfect matching is always possible.

The current method must be adapted to the surface code due to its non-periodic boundaries; an error on the boundary or a chain of errors leading to the boundary will generate only one terminal whence no perfect matching is possible. The extension is illustrated in figure 8. First, we determine the closest boundary to each terminal. For each node in the original graph, we create a unique boundary node. An edge between a node and its boundary represents an error chain stemming from the closest boundary, and is weighted accordingly. If our extension were stopped here, one would quickly observe that the only perfect matching possible is each node connected to its own boundary, which has dire consequences. To remedy this, all boundary nodes are inter-connected by weight-0 edges, so that when two nodes are matched, their respective boundaries can also be matched with no penalty.

Though we have only discussed space-like boundaries, in practice we cannot extract the final syndrome exactly. One can take this into account by introducing time-like boundaries. Note that there is still only one boundary node per terminal; the edge connecting a node to its boundary now takes the lower weighted choice between space and time boundaries.

The modification of the graph due to the boundaries in this manner gives rise to interesting optimizations. First and foremost, it permits the exclusion of highly weighted edges without fear of loss of the minimum-weight perfect matching (figure 9); only when it is less costly to join two nodes together (weight w) than each to their respective boundaries (weight $a + b$) must the former be considered. This condition discards only edges that we know from the geometry of the situation cannot be in the minimum-weight matching, allowing one to match a less highly connected graph than initially constructed. The case where $w = a + b$ is ambiguous and applying the optimization means we always prefer to match the nodes individually to their boundaries than to other nodes when the probabilities are equal. The optimization itself does not affect the weight-sum of the minimum-weight matching, hence it is *not* an approximation.

This optimization is of particular interest in the low physical error rate limit, where the terminals are so sparse that the graph breaks down into independent components. Each graph component can be matched independently. This in effect simplifies the global optimization problem to several local problems. The independence of graph components ensures the task can be easily parallelized, though we have not taken this direction.

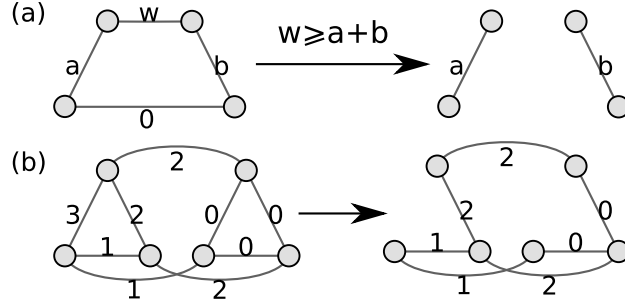


Fig. 9. (a) Optimization condition. Two nodes are connected to their boundaries by weight- a and weight- b edges respectively. If the edge joining the two nodes together has weight $w \geq a + b$, it can be safely discarded without affecting the minimum-weight matching. (b) Optimization applied to the graph of figure 8c.

Furthermore, the time separation between the latest node in a graph and the current time ensures that there exists a minimum edge weight connecting any node in that component to any future node. Once this minimum edge weight exceeds twice the distance to the boundary, the optimization condition will always be satisfied. The graph component becomes disconnected from all others; no more nodes or edges need to be added to it. Hence it can be matched, even as the quantum computation is running.

5 Time to failure simulation

Thus far we have discussed how syndrome information is extracted from the toric code and the surface code, and described an efficient implementation of the error correction procedure under both of these schemes. This forms the basis for our threshold error rate simulations.

The threshold error rate is derived from four processes: initialisation, readout, single-qubit gates (memory) and two-qubit gates (controlled-not). Each of these processes have an associated error rate and duration. In order to calculate a threshold, we assume that these parameters are equal across all four processes. That is, when we initialize a qubit to the $|0\rangle$ or $|+\rangle$ state, there is a probability p that the qubit is accidentally prepared into the $|1\rangle$ or $|-\rangle$ state respectively. Similarly, a readout error in either the X or the Z basis will yield the incorrect result with the same probability p . A memory error is the application of X , Y or Z , each with probability $p/3$ to an idle qubit. A two-qubit gate error is the application of one of the 15 nontrivial tensor products of I , X , Y and Z , each with probability $p/15$, after an ideal application of the two-qubit gate. Each of these processes are performed in one unit of time.

Our threshold calculation proceeds by assuming that we are given ahead of time some quantum state encoded in a distance- d code (either toric or surface code). The state begins in the simultaneous $+1$ eigenstate of all the stabilizers. Given such a state, we can determine the average time the state is sustained, using the described error correction procedure, before a logical failure: at each step, all the data qubits are time-evolved, and the syndrome extracted, which permits the surface to be error corrected. This cycle repeats until logical failure ensues. The simulations are performed by tracing the propagation of errors through the computer, not the entire quantum state.

For ideal syndrome extraction, instead of simulating time to failure directly, we also count the number of k -error failures and determine the logical error rate per timestep (the reciprocal

of time to failure), using

$$p_L^{(d)}(p_0) = \sum_{k=0}^Q A_d(k) p^k (1-p)^{(Q-k)}, \quad p = \frac{2}{3} p_0 \quad (1)$$

Here p_0 is the physical error rate, $Q(d)$ is the number of data qubits in the lattice, and $A_d(k)$ is the number of failure causing configurations as a result of k errors in the distance- d code. The factor of $\frac{2}{3}$ is due to our error model, as of the three possible errors X , Y , Z only two contain bit-flips which can lead to logical- X failures. Calculating A_d exactly is computationally intractable, however we can approximate it by randomly testing for failure only a fixed large number of the total number of configurations, $\binom{Q}{k}$, giving a failure ratio r_k and allowing the approximation $A_d \approx \binom{Q}{k} r_k$.

The results for both the toric code and surface code under ideal syndrome extraction are shown in figure 10. The data points are obtained directly from the time to failure simulations, whereas the curves are from counting the number of failures. Both codes show threshold values of $p_{\text{th}} = 0.155 \pm 0.005$. Our value obtained by direct simulation of the toric code is consistent with [21] which was obtained by mapping the problem onto a two-dimensional random-bond Ising model and identifying transitions between ordered phase and disordered phase. Their value of $p = 11\%$ for X (and Z) errors is recovered when we account for the factor of $\frac{2}{3}$ due to our single qubit error model. Differences thereafter may be attributed to different conventions when dangerous ambiguous syndromes arise.

The non-ideal syndrome extraction case is a little trickier as we assume that the final syndrome measurement is error free. This is resolved by assuming the current time t is the final step and extracting one more syndrome ideally. Should correction fail using this data, we record a failure time of t . Otherwise we continue to timestep $t + 1$, recollecting the syndrome using a non-ideal syndrome extraction cycle.

The results for the two codes now under non-ideal syndrome extraction are shown in figure 11. The toric code shows a threshold error rate of $p_{\text{th}} = 7.8 \times 10^{-3}$, coinciding with previously known results [12]. Slight differences in value may be attributed to the different methodologies of obtaining the threshold.

The surface code pseudo-thresholds fluctuate around the same region, part of which can be put down to the result of boundary effects. Because the boundary consists of only weight-3 stabilizers, syndrome qubits on the boundary are more reliable than those in the bulk. Thus the effective error rate per timestep (syndrome extraction cycle) is not uniform for different sized lattices; smaller lattices tend to be more reliable as the ratio of boundary to bulk qubits is large. By this rationale, one would expect to observe surface code pseudo-thresholds initially intersecting above the toric code threshold and then monotonically converging towards it. This monotonic trend is not observed once we approach distance-9, suggesting there is still more unexplained behaviour. Nevertheless, our results indicate that the asymptotic threshold for the surface code threshold is in the vicinity of the toric code.

Another difference between the two codes is the maximum number of errors that each can correct; a distance- d toric code can fail with $(d + 1)/2$ errors, whereas the surface code can fail with only $(d - 1)/2$ errors. This is due to correlated errors during the syndrome extraction circuit. One can find explicit examples where a single error during syndrome extraction in the surface code appears naïvely as two errors, thus causing failure in a distance-3 code. The

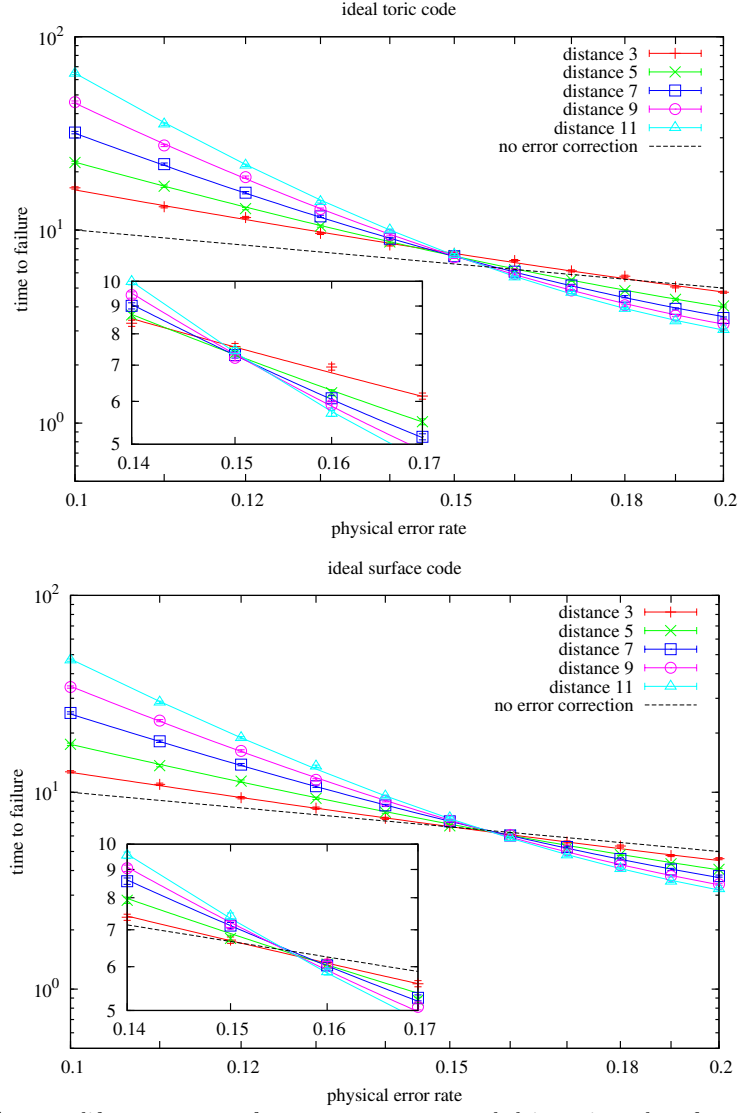


Fig. 10. Average life expectancy of a quantum state encoded in toric and surface codes under error free syndrome extraction. The error bars represent the standard deviation in the value of the average. The threshold is taken to be the error rate at the intersection between successive distance codes, $p_{\text{th}} = 0.155 \pm 0.005$.

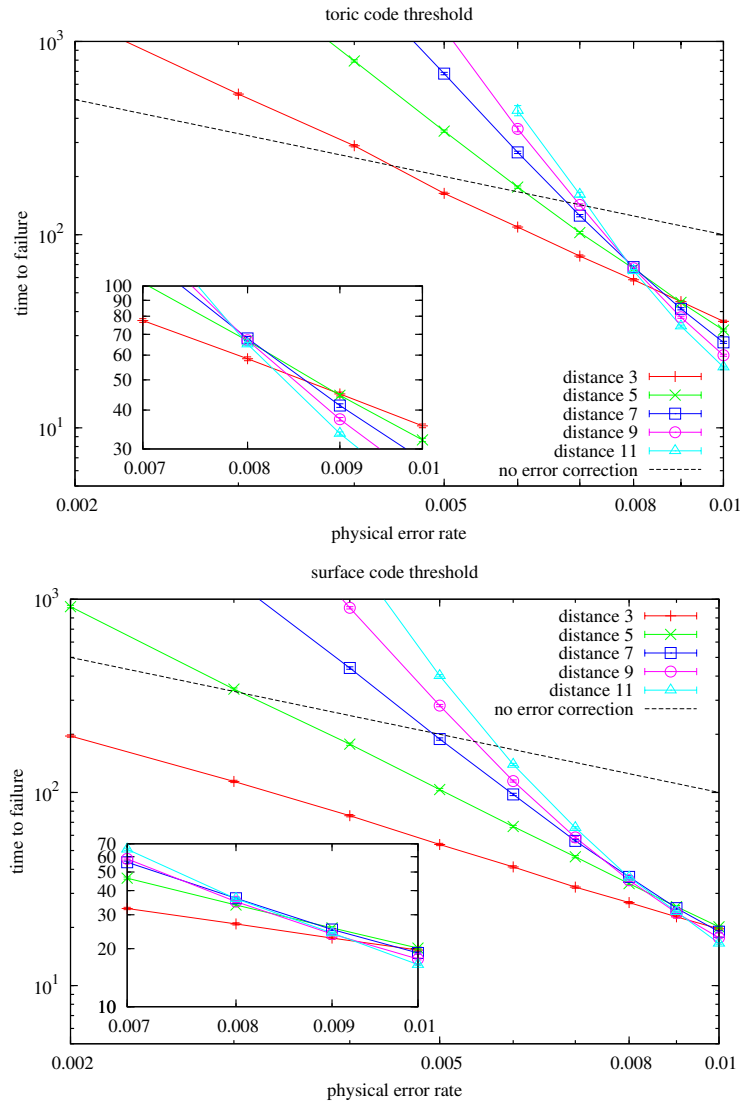


Fig. 11. Average life expectancy of a quantum state encoded in toric and surface codes using syndrome extraction circuits of figure 5. The toric code threshold is $p_{th} = 7.8 \times 10^{-3}$, and the surface code threshold is expected to follow similarly. Notice also that the surface code now corrects one fewer error than the toric code for the same distance code.

toric code, as a result of its wrap-around boundaries and hence somewhat redundant extra row of syndrome qubits, avoids this behaviour.

6 Conclusion

We have described an efficient error correction scheme implementable in practice. Using this graphical approach for error correction, we find the toric code threshold is $p_{\text{th}} = 7.8 \times 10^{-3}$. The surface code also shows a similar threshold. Further improvements to the graphical approach — such as changing the space-like and time-like edge weights to accurately reflect the relative probabilities of data and readout errors, or considering more error chains — would boost the performance of these codes in real life.

Error correction is usually thought of as performing this matching algorithm only when necessary, for example when encountering non-Clifford gates, after accumulating syndrome information over a long stretch of time. This delayed error correction means one must build and match a large graph, which can potentially become a bottleneck. However, even without introducing approximations, the graph can break into independent components thus the problem becomes highly parallelisable. Furthermore, it is possible to identify and match many disconnected graph components before encountering these non-Clifford gates, thus reducing the size of the task when one is finally forced to error correct.

Acknowledgements

We thank Charles Hill, and Zachary Evans for their helpful suggestions. This work was supported by the Australian Research Council, the Australian Government, and the US National Security Agency (NSA) and the Army Research Office (ARO) under contract number W911NF-08-1-0527.

References

1. R. Raussendorf, J. Harrington, and K. Goyal. Topological fault-tolerance in cluster state quantum computation. *New J. Phys.*, 9:199, 2007. quant-ph/0703143.
2. M. A. Nielsen and I. L. Chuang. *Quantum Computation and Quantum Information*. Cambridge University Press, Cambridge, 2000.
3. P. W. Shor. Algorithms for quantum computation: Discrete logarithms and factoring. In *Proc. 35th Annual Symposium on Foundations of Computer Science*, pages 124–134, 1994.
4. L. K. Grover. A fast quantum mechanical algorithm for database search. In *Proc. Twenty-Eighth Annual ACM Symposium on the Theory of Computing*, pages 212–219, 1996. quant-ph/9605043.
5. P. W. Shor. Scheme for reducing decoherence in quantum computer memory. *Phys. Rev. A*, 52:R2493, 1995.
6. A. R. Calderbank and P. W. Shor. Good quantum error-correcting codes exist. *Phys. Rev. A*, 54(2):1098–1105, 1996. quant-ph/9512032.
7. A. M. Steane. Multiple particle interference and quantum error correction. *Proc. R. Soc. Lond. A*, 425:2551–2576, 1996. quant-ph/9601029.
8. E. Knill, R. Laflamme, and W. H. Zurek. Accuracy threshold for quantum computation. Technical Report LAUR-96-2199, Los Alamos National Laboratory, 1996. quant-ph/9610011.
9. E. Knill. Quantum computing with realistically noisy devices. *Nature*, 434:39, 2005. quant-ph/0410199.
10. A. M. Stephens and Z. W. E. Evans. Accuracy threshold for concatenated error detection in one dimension. *arXiv:0902.2658*, 2009.

11. A. Yu. Kitaev. Fault-tolerant quantum computation by anyons. *quant-ph/9707021*, 1997.
12. R. Raussendorf and J. Harrington. Fault-tolerant quantum computation with high threshold in two dimensions. *Phys. Rev. Lett.*, 98:190504, 2007. [quant-ph/0610082](#).
13. A. G. Fowler, A. M. Stephens, and P. Groszkowski. High threshold universal quantum computation on the surface code. *arXiv:0803.0272*, 2008.
14. K. M. Svore, D. DiVincenzo, and B. Terhal. Noise threshold for a fault-tolerant two-dimensional lattice architecture. *Quant. Info. Comp.*, 7:297, 2007. [quant-ph/0604090](#).
15. F. M. Spedalieri and V. P. Roychowdhury. Latency in local, two-dimensional, fault-tolerant quantum computing. *arXiv:0805.4213*, 2008.
16. S. B. Bravyi and A. Y. Kitaev. Quantum Codes on a Lattice with Boundary. *Quantum Computers and Computing*, 2(1):43–48, 2001. [quant-ph/9811052](#).
17. G. S. Agarwal. Mesoscopic superpositions of states—approach to classicality and diagonalization in coherent state basis. *quant-ph/9810052*, 1998.
18. M. F. Freedman and D. A. Meyer. Projective plane and planar quantum codes. *quant-ph/9810055*, 1998.
19. J. Edmonds. Paths, trees, and flowers. *Canadian Journal of Mathematics*, 17(3):449–467, 1965.
20. W. Cook, A. Rohe, and Universität Bonn. *Computing Minimum-Weight Perfect Matchings*. Rheinische Friedrich-Wilhelms-Universität Bonn, 1997.
21. E. Dennis, A. Kitaev, A. Landahl, and J. Preskill. Topological quantum memory. *J. Math. Phys.*, 43:4452–4505, 2002. [quant-ph/0110143](#).